Proceedings of the 5th World Congress on Mechanical, Chemical, and Material Engineering (MCM'19)
Lisbon, Portugal – August 15 – 17, 2019
Paper No. HTFF 136
DOI: 10.11159/htff19.136

Natural Convection from Locally Heated Horizontal Rectangular Plate-Fin Heat Sinks

Shwin-Chung Wong, Yi-Cheng Lin, Hong-Jyun Liou
Department of Power Mechanical Engineering/National Tsing Hua University
101, 2nd Sec. Kuan-Fu Rd., Hsin-Chu, Taiwan, R.O.C.
scwong@pme.nthu.edu.tw; b02502135@ntu.edu.tw; hlpss91074@gmail.com

Abstract **-** This work investigates the characteristics and performance of natural convection from locally heated horizontal rectangular plate-fin heat sinks using 3-D unsteady numerical analysis. Different fin lengths (L = 128 or 254 mm), fin heights (H = 38 or 45 mm), heat fluxes (q = 0.9 or 1.8 W/cm^2), and heater positions (symmetric or asymmetric heating) are examined. For these long heat sinks, oscillating sliding-chimney plume always prevails to yield oscillating heat transfer coefficients. For each case, the time-averaged overall heat transfer coefficient $\bar{h}$ and the averaged base plate temperature $\bar{T}_b$ are calculated. The $\bar{T}_b$ is then used as the input uniform temperature to obtain the equivalent time-averaged overall heat transfer coefficient $\bar{h}_{eq}$. For all the investigated cases, $\bar{h}_{eq}$ differs from $\bar{h}$ by less than 4%. This means that $\bar{h}$ for a locally heated condition may be equivalently obtained employing empirical Nu correlations derived for uniform-temperature horizontal heat sinks, as long as the average base temperature $\bar{T}_b$ is used.

Keywords**:** Natural convection, plate fin heat sink, horizontal heat sink, sliding-chimney plume.

1. Introduction

Natural convection from rectangular plate-fin heat sinks has been intensively studied in response to its wide application on the thermal management of electronic devices and LED lamps. To focus on the effects of various geometric parameters, such as the length, height, spacing, and width (or fin number) of the fins, the heating conditions have almost always been uniform in temperature or heat flux. The empirical Nusselt number (*Nu*) correlations for heat transfer performance have been all derived for conditions with uniform base-plate temperature. In actual applications, however, the heat sinks are locally heated by single or multiple sources so that the base-plate temperatures are highly non-uniform. To our knowledge, only Von de Pol and Tierney [1] mathematically handled locally heated vertical heat sinks with a heat source positioning at the middle of the heat sink base plate. Considering a vertical heat sink as a series of adjacent, U-shaped channels, the thermal dissipations from each of the channels, at respective approximate average temperatures, were determined using the empirical *Nu* correlation associated with U-shaped channels. The average temperatures of the individual channels were obtained through iteration based on one-dimensional conduction in the base and simplified energy-balance of the entire heat sink. The model predictions of the heat source temperature agreed well with experimental results for a variety of heat sink sizes. According to the work of Von de Pol and Tierney [1], the *Nu* correlations derived from uniform-temperature conditions may be used to approximately estimate the thermal performance of a heat sink with non-uniform base-plate temperatures, if the average temperature of each individual channel can be obtained. However, this method has not been followed up with further detailed investigation or verification. Clear guidance is needed for how to apply the uniform-temperature *Nu* correlations to actual situations with large temperature variations. The present study aims to provide such a guidance. Horizontal rectangular plate-fin heat sinks are considered because they are widely used for electronics cooling and their flow characteristics are more complex than vertical heat sinks. The following is a literature survey on natural convection from horizontal rectangular plate-fin heat sinks.

Harahap and McManus [2] were the pioneers to observe different flow patterns associated with horizontal rectangular plate-fin heat sinks with different fin heights (L = 127 and 254 mm) and spacings (S = 6.4 and 8 mm). For short L (127 mm) with large Hs (25 and 38 mm), a stable single-chimney plume was observed. For long L (254 mm) with small Hs (6.4 and 13 mm), sliding-chimney plumes appeared, sliding back and forth along the longitudinal direction. Jones and Smith [3] focused on the effect of S by testing long fin arrays with a fixed length L = 254 mm. The data show that the time-averaged

overall convection heat transfer coefficient $\bar{h}$ depends strongly on S but weakly on H. Considering S as the characteristic length of the Nu and the Gr, their empirical correlation presents good agreement with the experimental data. Leung et al. [4, 5] experimentally studied the effects of S, L, H, and ΔT, the temperature difference between the fin base and the environment, on the heat transfer rate. The S_{opt} was found to increase significantly with increasing L and decreasing H but decrease slightly with increasing ΔT [4]. Harahap and Setio [6] modified the correlations of Harahap and McManus [2], which adopts L as the characteristic length.

Other experiments dealt with short heat sinks with $L \leqq 100$ mm [7, 8], for which the stable single-chimney plume pattern prevails. For a fixed L = 100 mm, Yüncü and Anbar [8] indicated that the heat transfer rate strongly depends on the fin spacing and the number of fins for a given ΔT. The S_{opt} is insensitive to ΔT but decreases with increasing H. Mobedi and Yüncü [9] and Dialameh et al. [10] conducted 3-D numerical analysis for short heat sinks. Baskaya et al. [11] applied a 3-D steady-state numerical model to long horizontal fin arrays without considering the presence of unsteady sliding-chimney plumes.

The interesting finding of the sliding-chimney plumes under large L by Harahap and McManus [2] was carefully investigated by Huang and Wong [12] using a 3-D unsteady numerical analysis. The dynamic characteristics of the natural convection from horizontal rectangular heat sinks were explored for a wide range of L = 56−500 mm under a fixed S = 6.4 mm and two heights H = 6.4 and 38 mm. The developing process of the sliding-chimney plumes for long heat sinks was described in detail. When the airflow drawn in from the ambience is sufficiently heated in the midway toward the central region, air bulbs are lifted by buoyancy. Then, downward airflow from the upper ambience is induced and leads to local recirculation and the subsequent oscillatory sliding-chimney plume. In agreement with the experimental observations [2], the numerical results exhibit stable single-chimney plumes for short fins and the evolution of unsteady sliding-chimney plumes for L larger than about 100 mm. With the transient behavior properly managed, the numerical results exhibit good agreement with the empirical Nu correlations of Harahap and McManus [2] and Jones and Smith [3] for long heat sinks. Wong and Huang [13] further conducted parametric study for long heat sinks (L = 128, 254 and 380 mm) over wide ranges of H and S. The predicted dependence of S_{opt} on H and L agrees well with experimental results and is explained based on numerical results of flow and heat transfer characteristics.

After the pioneering work of Harahap and McManus [2], the flow and thermal mechanisms of natural convection from horizontal rectangular plate-fin heat sinks have now been clearly understood. However, all these studies pertain to conditions with a uniform heat sink base temperature. It is necessary to study how these empirical Nu correlations [2-6] can be applied in a proper manner to actual heat sinks with large temperature variations in the base plate. Following the way of previous numerical studies [9-13], only single fin channel is considered. The flow and thermal characteristics associated with locally heated fin channels will be numerically investigated. The average heat transfer coefficients and the average base plate temperatures will be obtained. Then, the average heat transfer coefficients corresponding to the uniform-temperature conditions with the average base plate temperatures will be obtained and compared with the results for the original locally heated conditions.

2. Theoretical Model

2.1. Computational Domain

For analysis of a locally heated heat sink channel, there is no symmetry benefit over the length of the heat sink except for the special case where the heater is placed in the middle. But if the heat flux is uniform across the channel width, symmetry holds with respect to the longitudinal mid-plane of the channel. In Fig. 1a, the computational domain includes the whole half channel and extension regions at both ends and above the channel. The solid phase includes a half fin and a half base plate of the channel. The total length, height and width of the computational domain are $3L$,$10H+\delta_b$, and $(S+\delta)/2$, where H, L, S, and δ, are the height, length, spacing and thickness of the fin, respectively, and δ_b is the base-plate thickness. When the heater is centralized, symmetric analysis may be used with the domain shown in Fig. 1b. The total height, length, and width of the computational domain are $1.5L$, $10H+\delta_b$, and $(S+\delta)/2$, respectively. For conditions with uniform base plate temperature, the base plate can be further excluded. The total height, length, and width of the computational domain are $1.5L$, $10H$, and $(S+\delta)/2$. Hexahedral mesh is adopted, as representatively shown in Fig. 2 for a symmetric and an asymmetric situation with L = 254 mm and H = 45 mm. Fine grids are used within the flow channel. Moreover, finest grids are formed

to treat the large gradients in the boundary layers adjacent to the solid surfaces. Grid independence tests on the flow channel of fin arrays have been conducted. The smallest grid size, adjacent to the channel wall, is selected to be 0.5 mm, as the resultant $\bar{h}$s differs from those obtained using a smallest size of 0.25 mm by only 0.2%. Domain independence tests have been conducted for symmetric situations. Accordingly, the extension height of 9H and extension length of L are selected. The grid numbers range from 443,941 for L = 128 mm and H = 38 mm with symmetric heating to 2,188,006 for L = 254 mm and H = 45 mm with asymmetric heating.

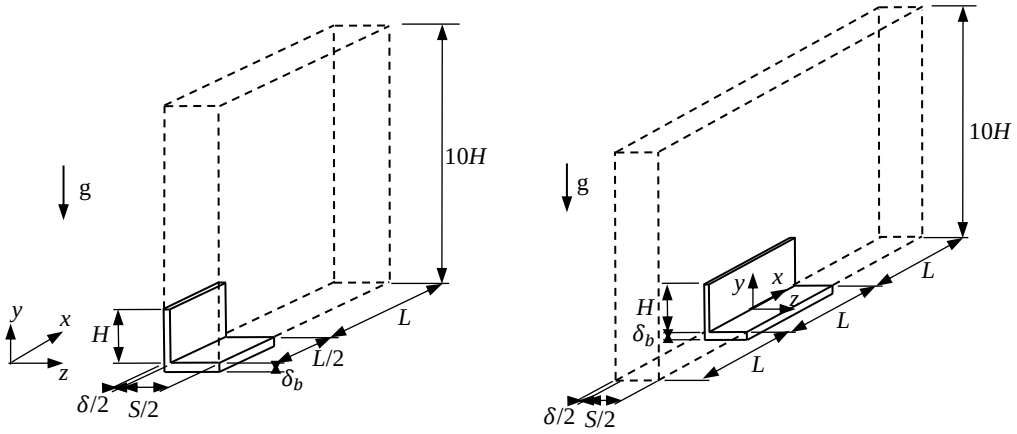

Fig. 1 Computational domain, (a) symmetric heating, (b) asymmetric heating.

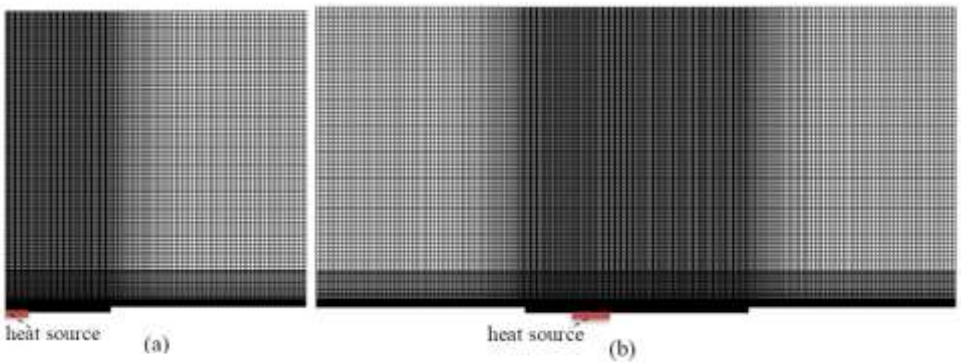

Fig. 2: Typical grid patterns (L=254mm, H=45 mm), (a) symmetric heating, (b) asymmetric heating.

2.2. Governing Equations

The following assumptions are made:

1. The flow field is incompressible laminar flow.
2. The Boussinesq approximation is assumed with the coefficient of thermal expansion $\beta = 1/T_\infty$ and the fluid density evaluated at T_∞ [14]. The other fluid properties are temperature-dependent by interpolating the data provided in [15].
3. The heat flux is uniform across the channel width.
4. Radiation heat loss is ignored.

For the gas phase:

Continuity equation:

$$\nabla \cdot \mathbf{V} = 0 \tag{1}$$

Momentum equations:

$$\frac{\partial u}{\partial t} + (\mathbf{V} \cdot \nabla)u = -\frac{1}{\rho_\infty}\frac{\partial p}{\partial x} + \nabla \cdot (\nu \nabla u), \tag{2}$$

$$\frac{\partial v}{\partial t} + (\mathbf{V} \cdot \nabla)v = -\frac{1}{\rho_\infty}\frac{\partial \hat{p}}{\partial y} + \nabla \cdot (\nu \nabla v) + g\beta(T - T_\infty), \tag{3}$$

$$\frac{\partial w}{\partial t} + (\mathbf{V} \cdot \nabla)w = -\frac{1}{\rho_\infty}\frac{\partial p}{\partial z} + \nabla \cdot (\nu \nabla w), \tag{4}$$

where ρ, ν and p are the density, kinematic viscosity and static pressure of air, respectively, $\mathbf{V} = u\mathbf{i}+v\mathbf{j}+w\mathbf{k}$, and $\hat{p} = p + \rho_\infty g y$.

Energy equation:

$$\frac{\partial T}{\partial t} + (\mathbf{V} \cdot \nabla)T = \nabla \cdot (\alpha \nabla T). \tag{5}$$

For the solid phase:

$$\frac{\partial T}{\partial t} = \nabla \cdot (\alpha_s \nabla T). \tag{6}$$

In Eqs. 5 and 6, α and α_s are the thermal diffusivity of air and aluminium alloy, respectively. The thickness of the aluminium fins is 1 mm, the base plate thickness is 6 mm, and the thermal conduction used in computations is 202.4 W/mK.

2.3. Boundary Conditions

The boundary conditions of the computational domain are shown in Fig. 1. In Fig. 1a, a uniform heat flux is applied to the heating area, while other area on the bottom surface is subjected to an adiabatic condition. Symmetric boundary conditions, $\frac{\partial u}{\partial y} = \frac{\partial v}{\partial y} = \frac{\partial w}{\partial y} = \frac{\partial T}{\partial y} = 0$, are applied at the longitudinal mid-channel plane and the transverse mid-plane of the channel. The top, side, and bottom surfaces of the extension region are open boundaries subjected to zero velocity derivatives in the normal direction. The no-slip condition is imposed on solid surface with

$$u = v = w = 0 \tag{7}$$

On fin and base surfaces,

$$T_w = T_a \tag{8}$$

$$k\frac{\partial T}{\partial n}\bigg|_w = k_a \frac{\partial T}{\partial n}\bigg|_a \tag{9}$$

where n is the normal direction of a surface.

The average base temperature $\bar{T}_b$ is determined as

$$\bar{T}_b = \frac{1}{A_b \tau}\iint T_b dA_b dt \tag{10}$$

where T_b is the temperature distribution over the bottom surface of the base plate, A_b is the surface area of the bottom surface, and τ is the time integration duration. The local heat transfer coefficient h is determined by

$$h(t) = \frac{q_w(t)}{T_w(t) - T_\infty} \tag{11}$$

where q_w and T_w are the local heat flux and temperature on the fin or the base wall, respectively. The average heat transfer coefficient over channel surface is

$$h_{avg}(t) = \frac{1}{A_w}\int \frac{q_w(t)}{T_w(t) - T_\infty} dA_w \tag{12}$$

The boundary conditions are similar in Fig. 1b, except for the symmetric conditions imposing on the vertical transverse mid-plane of the channel.

2.4. Numerical Method

The commercial software ANSYS Fluent v15.0 was utilized for solving the velocity and temperature fields. Conservation equations (1)–(5) were solved by a pressure based solver and coupled with the heat conduction equation (6). A first-order temporal discretization was adopted with truncation errors of O(Δt). The non-iterative PISO (Pressure-Implicit with Splitting of Operators) method [16] was adopted for unsteady simulation to speed up the transient simulation. The time step for computation was 0.002s, for which the results in $\bar{h}$ were different from those for a time step of 0.0002 s by only 0.25%. The maximum residuals for convergence were 10^{-4} for the continuity equation, 10^{-4} for the momentum equations, and 10^{-8} for the energy equations. To save the computational effort, steady-state simulation was first conducted, whose residuals could reach only about O(10^{-1}) or O(10^{-2}), and the steady-state results were used as the initial guesses for transient simulations.

For the present long heat sinks, the sliding-chimney plume yields an oscillating h_{avg} (t) history as shown in Fig. 3. To evaluate the time-averaged overall heat transfer coefficient $\bar{h}$ over the unsteady h_{avg} history, we follow the practice of Huang and Wong [12, 13], in which the $\bar{h}$ values are calculated over 20–30 s. In fact, different time-averaging durations have been tested: between 18–30 s, 20–30 s, or 22–30 s. The differences in $\bar{h}$ for different durations are found within only ±0.3%. Therefore, time averaging is made over the period between 20 s and 30 s as

$$\bar{h} = \int_{20s}^{30s} h_{avg}\,(t)dt. \tag{13}$$

For short heat sinks, the plume is steady-state if the heater is positioned at the center of the heat sink. In these cases, steady-state analysis without the transient terms is adopted.

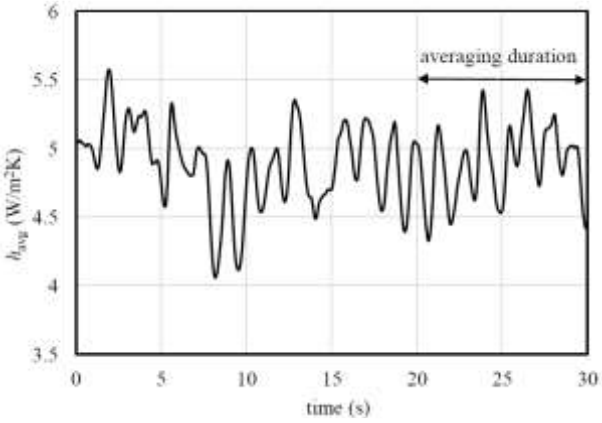

Fig. 3: History of $h_{avg}(t)$ for the channel with L=254mm, H=45 mm, and S=10mm under symmetric heating (q = 0.9 W/cm^2).

3. Results and Discussion

3.1. Symmetrical Heating

We first examined the cases with symmetric local heating. Two channel lengths (L = 128 or 254 mm) and two fin heights (H = 38 or 45 mm) are selected with fin spacing S = 10 mm, near the optimum fin spacing. The base plate thickness, and the fin thickness are fixed at 6 mm and 1 mm, respectively. The heater is 44 mm in length and 5.5 mm in half width. Two different heating fluxes, q = 0.9 or 1.8 W/cm^2, are imposed. The ambient temperature T_∞ is 20 ℃ (T_∞ = 293 K).

Fig. 4 displays an instantaneous temperature distribution of air flow over the longitudinal mid-plane of the channel (L = 254 mm, H = 45 mm, S = 10 mm) with symmetric heat flux q = 0.9 W/cm^2. For all present cases, strongly oscillating sliding-chimney flow prevails. For each case, the time-averaged fin-base temperature $\overline{T}_b$ is obtained. (It is noted that while the gas-phase temperature distributions oscillate significantly, the temperature distribution over the base plate appears rather stable.) This $\overline{T}_b$ is then used as the equivalent uniform base temperature to evaluate the equivalent overall heat transfer coefficient $\overline{h}_{eq}$. Table 1 lists the original $\overline{h}$, the average base temperature $\overline{T}_b$, the equivalent $\overline{h}_{eq}$ at $\overline{T}_b$, and the percent difference between $\overline{h}$ and $\overline{h}_{eq}$ for various cases under q = 0.9 W/cm^2. It can be seen that the differences between $\overline{h}$ and $\overline{h}_{eq}$ are less than ±1.52%. Table 2 compares $\overline{h}$ and $\overline{h}_{eq}$ for q = 1.8 W/cm^2, showing differences within ±2.73%. It is noted that when q = 1.8 W/cm^2, $\overline{T}_b$s are so high that the Boussinesq approximation may not be suitable. But it is clear that, $\overline{h}_{eq}$ approximates $\overline{h}$ very well for all the above cases investigated.

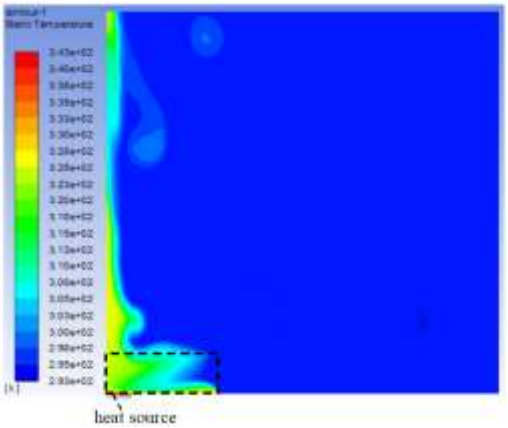

Fig. 4: Instantaneous air temperature distribution over the longitudinal mid-plane of the channel with L=254 mm, H=45 mm, and S=10 mm under symmetric heating (q = 0.9 W/cm^2).

Table 1: The differences between $\overline{h}$ and $\overline{h}_{eq}$ for different cases with symmetric heating (q = 0.9 W/cm^2).

	L=128 mm				L=254 mm			
	$\overline{T}_b$ (℃)	$\overline{h}$ (W/m^2 K)	$\overline{h}_{eq}$ at $\overline{T}_b$ (W/m^2 K)	difference in $\overline{h}$ and $\overline{h}_{eq}$	$\overline{T}_b$ (℃)	$\overline{h}$ (W/m^2 K)	$\overline{h}_{eq}$ at $\overline{T}_b$ (W/m^2 K)	difference in $\overline{h}$ and $\overline{h}_{eq}$
H=38mm	87.66	6.747	6.71	0.55%	69.93	3.95	3.98	-0.75%
H=45mm	78.03	5.83	5.73	1.75%	64.66	4.02	3.96	1.52%

Table 2: The differences between $\overline{h}$ and $\overline{h}_{eq}$ for different cases with symmetric heating (q = 1.8 W/cm^2).

	L=128 mm				L=254 mm			
	$\overline{T}_b$ (℃)	$\overline{h}$ (W/m^2 K)	$\overline{h}_{eq}$ at $\overline{T}_b$ (W/m^2 K)	difference in $\overline{h}$ and $\overline{h}_{eq}$	$\overline{T}_b$ (℃)	$\overline{h}$ (W/m^2 K)	$\overline{h}_{eq}$ at $\overline{T}_b$ (W/m^2 K)	difference in $\overline{h}$ and $\overline{h}_{eq}$
H=38mm	133.30	5.618	5.624	-0.11%	101.74	4.89	4.76	2.73%
H=45mm	121.32	6.69	6.674	0.24%	92.53	4.74	4.75	-0.21%

3.2. Asymmetric Local Heating

The cases with asymmetric local heating are also examined for different conditions. The center of the heating zone is shifted from the center of the channel by 44 mm. Fig. 5 presents the instantaneous temperature distribution of air flow over the longitudinal mid-plane of the channel (L = 254 mm, H = 45 mm, S = 10 mm) with asymmetric heat flux q = 0.9 W/cm^2. Fig. 6 illustrates the non-uniform longitudinal temperature distribution on the bottom surface of the base plate, as well as its average temperature $\bar{T}_b$ adopted to calculate the corresponding $\bar{h}_{eq}$. Tables 3 and 4 compare $\bar{h}$ and $\bar{h}_{eq}$ for asymmetric heating with q = 0.9 W/cm^2 and 1.8 W/cm^2, respectively. The maximum differences are about 4%.

These results for various conditions indicate that the heat transfer coefficient for a locally heated condition may be equivalently obtained employing current empirical *Nu* correlations, commonly derived for uniform-temperature horizontal heat sinks, as long as the average base temperature is used. More work will be done to consider the temperature variation over the whole multi-channel heat sink with heat spreading in the base plate is accounted for.

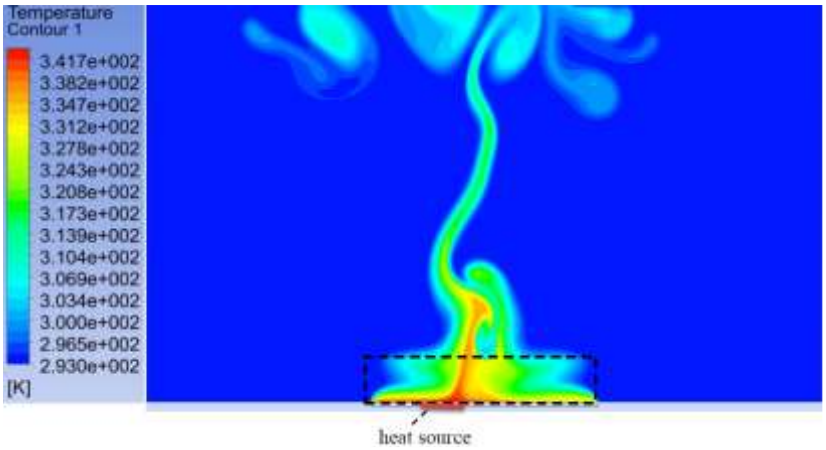

Fig. 5: Instantaneous air temperature distribution over the longitudinal mid-plane of the channel with L=254mm, H=45 mm, and S=10mm under asymmetric heating (q = 0.9 W/cm^2).

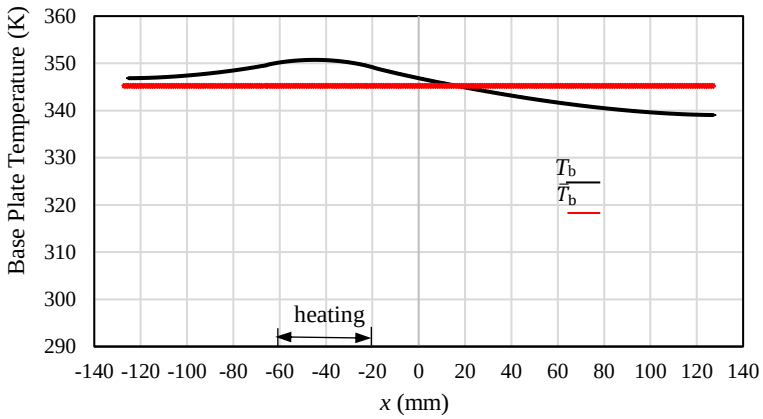

Fig. 6: Base plate temperature distribution (T_b) and average base temperature $\bar{T}_b$ for L=254mm, H=45 mm, and S=10mm under asymmetric heating (q = 0.9 W/cm^2).

Table 3: The differences between $\bar{h}$ and $\bar{h}_{eq}$ for different cases with asymmetric heating (q = 0.9 W/cm^2).

	L=128 mm				*L*=254 mm			
	$\bar{T}_b$ (℃)	$\bar{h}$ (W/m^2 K)	$\bar{h}_{eq}$ at $\bar{T}_b$ (W/m^2 K)	difference in $\bar{h}$ and $\bar{h}_{eq}$	$\bar{T}_b$ (℃)	$\bar{h}$ (W/m^2 K)	$\bar{h}_{eq}$ at $\bar{T}_b$ (W/m^2 K)	difference in $\bar{h}$ and $\bar{h}_{eq}$
H=38mm	89.04	5.786	5.78	0.10%	72.2	3.44	3.386	1.59%
H=45mm	81.72	5.81	5.584	4.05%	63.65	3.71	3.76	-1.33%

Table 4: The differences between $\bar{h}$ and $\bar{h}_{eq}$ for different cases with asymmetric heating (q = 1.8 W/cm^2).

	L=128 mm				*L*=254 mm			
	$\bar{T}_b$ (℃)	$\bar{h}$ (W/m^2 K)	$\bar{h}_{eq}$ at $\bar{T}_b$ (W/m^2 K)	difference in $\bar{h}$ and $\bar{h}_{eq}$	$\bar{T}_b$ (℃)	$\bar{h}$ (W/m^2 K)	$\bar{h}_{eq}$ at $\bar{T}_b$ (W/m^2 K)	difference in $\bar{h}$ and $\bar{h}_{eq}$
H=45mm	124.13	6.88	6.609	4.1%	94.08	4.54	4.607	-1.45%

4. Concluding Remarks

The characteristics and performance of natural convection from locally heated horizontal rectangular plate-fin heat sinks are investigated using 3-D unsteady numerical analysis. Different fin lengths (L = 128 or 254 mm), fin heights (H = 38 or 45 mm), heat fluxes (q = 0.9 or 1.8 W/cm^2), and heater positions (symmetric or asymmetric heating) are examined. For these long heat sinks, oscillating sliding-chimney plume always prevails to yield oscillating heat transfer coefficients. For each case, the time-averaged overall heat transfer coefficient $\bar{h}$ and the averaged base plate temperature $\bar{T}_b$ are calculated. The $\bar{T}_b$ is then used as the input uniform temperature to obtain the equivalent time-averaged overall heat transfer coefficient $\bar{h}_{eq}$. For all the investigated cases, $\bar{h}_{eq}$ differs from $\bar{h}$ by less than 4% even though the temperature distributions over the base plate are non-uniform. This means that $\bar{h}$ for a locally heated condition may be equivalently obtained employing empirical *Nu* correlations derived for uniform-temperature horizontal heat sinks, as long as the average base temperature $\bar{T}_b$ is used.

References

[1] D.W. Van de Pol and J.K. Tierney, "Free Convection heat transfer from vertical fin-arrays," *IEEE Trans. Parts Hyb. Pack.*, vol. 10 (1974) 267-271.

[2] F. Harahap and H.N. McManus Jr., "Natural convection heat transfer from horizontal rectangular fin arrays," *ASME J. Heat Transfer*, vol. 89, pp. 32-38, 1967.

[3] C.D. Jones and L.F. Smith, "Optimum arrangement of rectangular fins on horizontal surfaces for free-convection heat transfer," *ASME J. Heat Transfer*, vol. 92, pp. 6-10, 1970.

[4] C.W. Leung, S.D. Probert and M.J. Shilston, "Heat exchanger design: thermal performances of rectangular fins protruding from vertical or horizontal rectangular bases," *Appl. Energy*, vol. 20, pp. 123-140, 1985.

[5] C.W. Leung, S.D. Probert and M.J. Shilston, "Heat transfer performances of vertical rectangular fins protruding from rectangular bases: effect of fin length," *Appl. Energy*, vol. 22, pp. 313-318, 1986.

[6] F. Harahap and D. Setio, "Correlations for heat dissipation and natural convection heat-transfer from horizontally-based, vertically-finned arrays," *Appl. Energy*, vol. 69, pp. 29-38, 2001.

[7] C.B. Sobhan, S.P. Venkateshan and K.N. Seetharamu, "Experimental analysis of unsteady free convection heat transfer from horizontal fin arrays," *Wärme- und Stoffübertragung*, vol. 24, pp. 155-160, 1989.

[8] H. Yüncü and G. Anbar, "An experimental investigation on performance of rectangular fins on a horizontal base in free convection heat transfer," *Heat Mass Transfer*, vol. 33, pp. 507–514, 1998.

[9] M. Mobedi and H. Yüncü, "A three dimensional numerical study on natural convection heat transfer from short horizontal rectangular fin array," *Heat Mass Transfer*, vol. 39, pp. 267–275, 2003.

[10] L. Dialameh, M. Yaghoubi and O. Abouali, "Natural convection from an array of horizontal rectangular thick fins with short length," *Appl. Therm. Eng.*, vol. 28, pp. 2371–2379, 2008.
[11] S. Baskaya, M. Sivrioglu and M. Ozek, "Parametric study of natural convection heat transfer from horizontal rectangular fin arrays," *Int. J. Therm. Sci.*, vol. 39, pp. 797– 805, 2000.
[12] G.-J. Huang and S.-C. Wong, "Dynamic characteristics of natural convection from horizontal rectangular fin arrays," *Appl. Therm. Eng.*, vol. 42, pp. 81-89, 2012.
[13] S.-C. Wong and G.-J. Huang, "Parametric study on the dynamic behavior of natural convection from horizontal rectangular fin arrays," *Int. J. Heat Mass Transfer*, vol. 60, pp. 334-342, 2013.
[14] A. Bejan, *Convection Heat Transfer*, 4th Ed., Wiley, 2013.
[15] F.P. Incropera, D.P. DeWitt, T.L. Bergman, and A.S. Lavine, *Principle of Heat and Mass Transfer*, Wiley, 7th Ed, 2013.
[16] R.I. Issa, "Solution of the implicitly discretized fluid flow equations by operator-splitting," *J. Comput. Phys.*, vol. 62, pp. 40–65, 1986.